International Journal of Thermophysics (2022) 43:9
https://doi.org/10.1007/s10765-021-02931-9

Evaluating the Role of Sodium Dodecylbenzene Sulfonate as Surfactant Towards Enhancing Thermophysical Properties of Paraffin/Graphene Nanoplatelet Phase Change Material: Synthesis and Characterization in PV Cooling Perspective

Nurul Humaira Muhd Zaimi[1] · Amirjan Nawabjan[1] · Shaharin Fadzli Abd Rahman[2] · Siti Maherah Hussin[1] · Siti Nur Nashya Azlika Hamidon[1]

Received: 16 August 2021 / Accepted: 11 October 2021 / Published online: 2 November 2021

Abstract

Nanoparticles addition in the phase change material (PCMs) has been proved to improve its thermophysical properties. However, it also has been reported to cause agglomeration, which will counteract the thermophysical enhancement. The addition of surfactant to this matrix is believed to reduce the agglomeration. However, no comparison studies reported how the addition of surfactant in nano-enhanced phase-change material (NPCMs) improves its thermophysical properties and has assessed its performance in enhancing the temperature-reduction characteristics of PV panels under field-testing conditions. Hence, this work aims to experimentally evaluate the impact of adding surfactants to the NPCMs matrix to improve its morphological and thermophysical properties and evaluate its performance in outdoor conditions. Graphene nanoplatelet (GNP) with 1, 3, and 5 wt% (PG1, PG3, and PG5) was added to the paraffin wax (PW), followed by the addition of sodium dodecylbenzene sulfonate (SDBS) as the surfactant (PGS1, PGS3, and PGS5). Thermophysical properties such as latent heat, specific heat capacity, thermal conductivity, and total heat stored were investigated. The best improvement was shown by sample PGS5 (PW/5 wt% GNP with SDBS) with the performance of; (a) 43.2% improvement in latent heat, (b) 69.5% improvement in specific heat capacity, (c) 73.45% enhancement of heat transfer rate, (d) total heat stored with 64.13% improvement, and (e) relative enhancement by a factor of 25.94 in thermal conductivity. On-site evaluation on PV module also showed the reduction of temperature as high as 44.2%. All this proving the importance of SDBS to improve the thermophysical properties and suitability as a PV module coolant.

Keywords Nanoparticles · Phase change material · Photovoltaic · Surfactant · Thermophysical properties

1 Introduction

The generation of electricity using solar photovoltaic (PV) power is strongly influenced by the irradiance level and the panel's temperature. The latter constitutes a primary challenge to PV operation, especially in countries with hot climates. A previous study showed that for every 1 °C increment in operating temperature, the amount of PV electricity generated is reduced by as much as 0.4% [1]. Despite the effectiveness of methods such as water sprinklers [2], forced ventilation [3], and high ventilation [4] in cooling panels, these approaches require high capital outlays and are expensive to maintain in terms of water and electricity consumption. In addition, long-term exposure to humidity can lead to corrosion in systems that use water-based sprinklers, thereby shortening the life span of the panels.

Phase-change materials, PCMs [5–13] offer a cheaper alternative as coolants for PV modules. In addition, PCMs also easily scalable, offering added advantage of covering big surface areas without occurring huge cost. Not to mention it is easier to maintain for a longer period. Moreover, PCMs are abundantly available and cheap, and they can be easily obtained, ensuring economic viability and market penetration [14].

However, PCMs alone have several undesirable thermal characteristics and are generally characterized by low specific heat capacities [15], low thermal conductivities [16], and latent heat, which contradict with characteristics to act as good coolant material for PV modules. To improve the properties of existing PCMs, they are often combined with other materials such as microfin [14, 17–21], other types of PCMs [22], carbons [23], and nanoparticles (NPs). A PCMs that is blended with NPs is known as a nano-enhanced phase-change material (NPCMs). Examples of NPs used in NPCMs include graphene oxide (GO) [24], titanium oxide (TiO_2) [25], aluminum oxide (Al_2O_3) [26, 27], Fe_2O_3 [28], SiO_2 [27, 28], and ZnO [28]. Since the tiny NPs have larger surface-area-to-volume ratios, they foster the interaction of NPs with the PCMs, thus adjusting the PCM's thermal properties [29]. In addition, NPCMs have been proven to enhance panel performance by enhancing their thermophysical properties. However, despite these advantages, the use of NPCMs was reported to cause agglomeration, a phenomenon in which NPs cluster and suspend together, thereby increasing the effective size of the NPs. After several melting–solidification thermal cycles (increased hours of operation), this severe agglomeration will ultimately lead to reliability issues in NPCMs. Therefore, it is important to avoid agglomeration as it can degrade the thermophysical properties of NPCMs, making them less effective in reducing PV module temperature.

To mitigate the agglomeration problem, surfactants can be added to the NPCMs matrix [30, 31], producing so-called surfactant-added NPCMs (SNPCMs), as shown in Fig. 1. As a result, the surface tension between the NPs and the PCMs is reduced, making the PCMs and NPs disperse better, reduce the agglomeration, and in turn improve their thermophysical properties. However, despite the various studies reported on the usage of SNPCMs with several different characterizations,

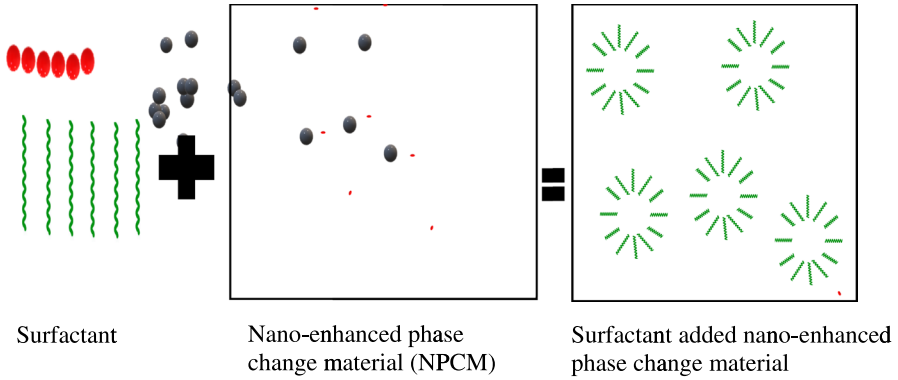

Fig. 1 Surfactant added nano-enhanced phase change material

as shown in Table 1, there are no comparison studies reported on how the addition of surfactant in NPCMs matrix plays a role in improving its thermophysical properties. Moreover, no studies have assessed its performance in enhancing the temperature-reduction characteristics of PV panels under field-testing conditions. Therefore, it is important to analyze the role of sodium dodecyl-benzene sulfonate (SDBS) in enhancing the thermophysical properties of the NPCMs to ensure the best formula in cooling PV panels, which can offer not only significant advantages of the simpler method without the need for any controlled environment but also a cost-effective approach for long term reliability of PV modules. This research work will focus exactly on that. First, NPCMs will be synthesized using graphene nanoplatelets (GNPs) as NPs of interest and paraffin wax (PW) as PCMs. Followed by the addition of SDBS to produce SNPCMs. This work aims to synthesize and characterize SNPCMs, which are physically stable and chemically with improved thermophysical properties to act as PV module coolants. Furthermore, the samples will also be subjected to on-site evaluation to investigate the practical aspect of acting as PV module coolant, highlighting the significance of current research work.

The current manuscript is presented as follows; the fabrication of NPCMs, SNPCMs, and experimental procedure will be explained in Sect. 2. The samples' morphology and various effect on thermophysical properties (charging and discharging rate, melting and solidifying temperature, latent heat, specific heat capacity, thermal conductivity, and total heat stored) are covered in Sect. 3. Finally, the conclusion will be discussed in Sect. 4.

2 Materials and Methods

2.1 Chemicals Used

PW was chosen as base PCM material due to its characteristics such as: (a) non-corrosive and non-toxic nature, (b) lack of sub-cooling, and (c) and high heat

Table 1 Selection of studies involving the use of surfactants

References	Years	PCM	NP	Surfactant	NP's weight (wt%)	Characterization	Comparison of thermophysical properties between NPCM and SNPCM	Integration of material for real-time application
[24]	2020	Paraffin wax	GO	Sodium dodecylbenzene sulfonate (SDBS)	0.3	Thermal conductivity	None	Yes/solar-still
[32]	2019	Water	Nano-SiC	Ammonium cetyl cetyl trichromyl ammonium bromide (CTAB), sodium dodecyl sulfate (SDS), tannic acid + ammonia solution, sodium dodecylbenzene sulfonate (SDBS), sodium deoxycholate	3	Density, viscosity, thermal conductivity, suspension stability	Yes	Yes/photovoltaic-thermal system
[33]	2019	Ethylene glycol	Al_2O_3	Polyvinylpyrrolidone (PVP), Sodium dodecyl sulfate (SDS)	1	Morphology, thermal conductivity, viscosity, stability time	Yes	None
[34]	2018	Butyl stearyl	Carbon nanotubes (CNT)	Triton X-100, 1-decanol, sodium dodecyl sulphate, tetramethyl ethylene diamine	1, 2, 3, 4, 5	Latent heat, melting point, freezing point, stability time, thermal conductivity	None	None
[26]	2018	Paraffin wax	Al_2O_3, MWNCT, GNP	Sodium oleate, octadecylamine	0.5, 2	Thermal conductivity, stability observation	Yes	None

Table 1 (continued)

References	Years	PCM	NP	Surfactant	NP's weight (wt%)	Characterization	Comparison of thermophysical properties between NPCM and SNPCM	Integration of material for real-time application
[25]	2017	Paraffin wax	TiO_2	Sodium stearoyl lactylate (SSL)	0.5, 0.7, 1, 2, 3, 4	Morphology, latent heat, melting point, thermal stability, thermal conductivity	Yes	None
[35]	2016	Palmitic acid	TiO_2	Sodium dodecylbenzene sulfonate (SDBS)	0.5, 1, 3, 5	Morphology, latent heat, melting temperature, thermal stability, thermal reliability, thermal conductivity	None	None
[36]	2016	Paraffin wax	Al_2O_3	Sodium stearoyl lactylate (SSL)	2.5, 5, 7.5, 10	Charging and discharging rate, thermal conductivity, phase change temperature, latent heat, thermal reliability	None	None
[37]	2015	Paraffin wax	Nano magnetite	Oleic acid	10, 20	Morphology, latent heat, thermal conductivity	None	None
[28]	2015	Paraffin wax	Al_2O_3, Fe_2O_3 and SiO_2, ZnO	Sodium dodecyl sulfate (SDBS), cetyltrimethylammonium bromide (CTAB)	2, 4, 6, 8	Morphology, phase change temperature, latent heat, thermal conductivity, thermal diffusivity	None	None

Table 2 Properties of paraffin wax and nanoparticles were used in this study

Thermophysical property	Paraffin wax	GNP	SDBS
Manufacturer	Rubitherm	Sigma Aldrich	Sigma Aldrich
Melting temperature (°C)	35	N/A	N/A
Specific heat capacity ($kJ{\cdot}kg^{-1}{\cdot}K^{-1}$)	2	N/A	N/A
Thermal conductivity ($W{\cdot}m^{-1}{\cdot}K^{-1}$)	0.2	3000	N/A
Latent heat ($kJ{\cdot}kg^{-1}$)	160	N/A	N/A
Density ($kg{\cdot}m^{-3}$)	0.86	2.3	0.18

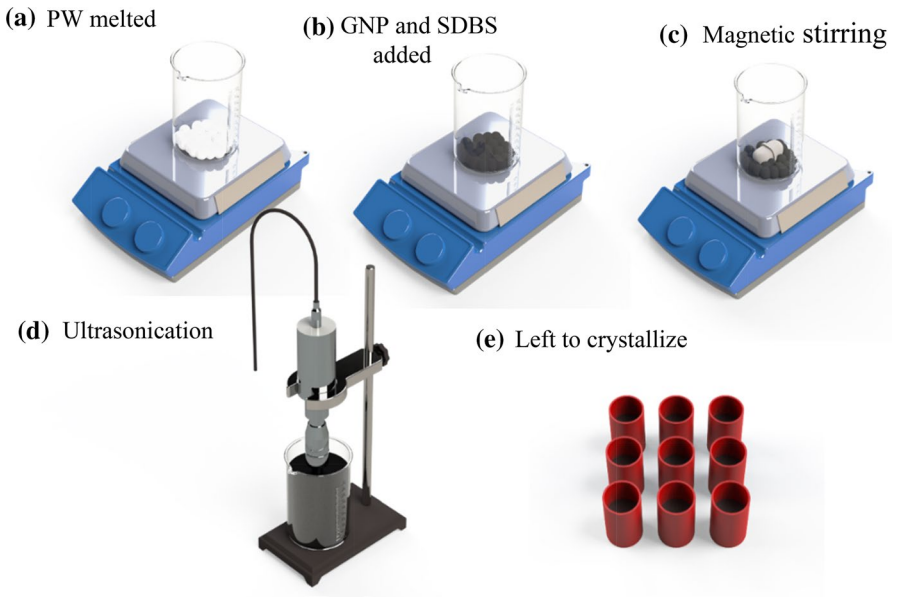

Fig. 2 Schematic representation of SNPCMs synthesis

capacity and latent heat. In addition, PW can store and release large amounts of latent heat energy while transitioning from a solid to a liquid and remains at a constant temperature throughout a phase change [38]. PW was purchased from Rubitherm with properties as shown in Table 2. The NPs used were GNP with an average particle size of 137 nm supplied by Sigma Aldrich. SDBS is an anionic surfactant, while GNP is a cationic NP, which leads to more stable dispersion when an oppositely charged surfactant and NPs are used [39]. The characteristics of PW, GNP, and SDBS are summarised in Table 2.

2.2 Fabrication of NPCMs, and SNPCMs

Figure 2 shows a schematic representation of the SNPCMs synthesis process. Samples were fabricated via a two-step process comprised of stirring and ultra-sonication [40], in which various proportions of GNP and SDBS were added. The process starts with 20 g of PW placed in a beaker to melt at 60 °C using a hot plate. Followed by the addition of GNP at three weight percentages (1, 3, and 5 wt%, respectively) and stirred for 15 min (NPCMs synthesis). SDBS is then added to some of the samples with a 1:1 ratio to produce SNPCMs samples. These samples will then undergo an ultrasonication process for better dispersion of GNP and SDBS and finally be left to crystallize at room temperature for one night. The final prepared samples were then labeled by the specification as listed in Table 3.

2.3 Morphological Analysis and Physical Observation

Physical observation and morphological analysis were performed to investigate and observe the sedimentation and agglomeration of the NPCMs sample. The physical and morphological elements of the sample can affect the performance of the NPCMs. The NPCMs and SNPCMs samples were analyzed using FESEM (model Carl-Zeiss Supra 35VP FESEM) and observed using a digital camera. The morphological study was used to observe the dispersion of GNP in PW, followed by an investigation of the agglomeration effect when SDBS is added to this matrix. Samples were coated in platinum using a platinum sputter coater under vacuum pressure for 1 min at a current of 20 mA and a voltage of 1.6 kV to provide electrical conductivity and prevent the surface charge accumulation. The samples were then examined at 10 kV of acceleration voltage. After the samples were prepared, the material was left to solidify, and its physical behavior was observed using a DSLR camera.

2.4 Thermophysical Characterization

Each sample's charging and the discharging rate was analyzed by measuring the time taken for each sample to melt and solidify. Next, the hot plate was heated to 50 °C, and each of the samples was placed on it until it was completely melted.

Table 3 Compositions of fabricated paraffin wax samples

Sample	Composition	Type
PW	Paraffin wax	PCM
PG1	Paraffin wax with 1 wt% GNP	NPCM
PG3	Paraffin wax with 3 wt% GNP	NPCM
PG5	Paraffin wax with 5 wt% GNP	NPCM
PGS1	Paraffin wax with 1 wt% GNP and SDBS	SNPCM
PGS3	Paraffin wax with 3 wt% GNP and SDBS	SNPCM
PGS5	Paraffin wax with 5 wt% GNP and SDBS	SNPCM

Samples were then allowed to crystallize at room temperature, and the time taken for it to solidify was recorded.

The melting/solidification temperatures, latent heat, and specific heat capacity of each sample were measured using a differential scanning calorimeter (DSC1, Mettler Toledo, Canada) over two heating and cooling cycles applied to remove uneven sample heating and to generate actual data, respectively. All samples were heated from 30 to 60 °C at a rate of 5 °C·min^{-1} and cooled at the same rate. Sapphire served as an external standard for measuring the specific heat capacity. The samples and sapphire were heated separately over the same temperature range at the same heating and cooling rates.

To determine the thermal conductivity, this study analyses a steady-state method in which the thermal conductivity was measured when all the temperatures had remained constant over time. The measurement was taken using thermal conductivity apparatus [41]. The samples were prepared in a 0.0021 m^3 PVC mold to generate a cylindrical form, as shown in Fig. 3, and the base area of each was measured. Each sample was sandwiched between two stainless steel bars and placed between a heat chamber and a water-cooling system (Fig. 4). The heat chamber was then continuously heated to the stainless-steel bar at one end and cooled at the other by the water cooler. The stainless steel bar was thermally insulated; there will be no energy loss, thus making the heat throughout the bar Q_{bar} is the same as the heat through the sample, Q_{sample}, and is equal to the heat absorbed by the water cooler, Q_{bar} ($Q_{\text{bar}} = Q_{\text{sample}} = Q_{\text{w}}$). The thermal conductivity, κ (W·m^{-1}·K^{-1}), of each sample was

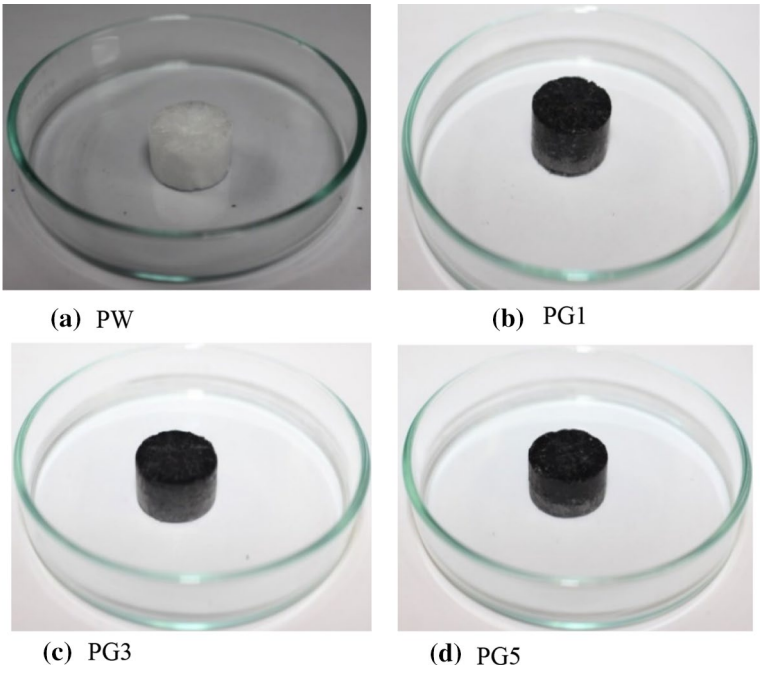

Fig. 3 (a)–(d) Samples for thermal conductivity measurement

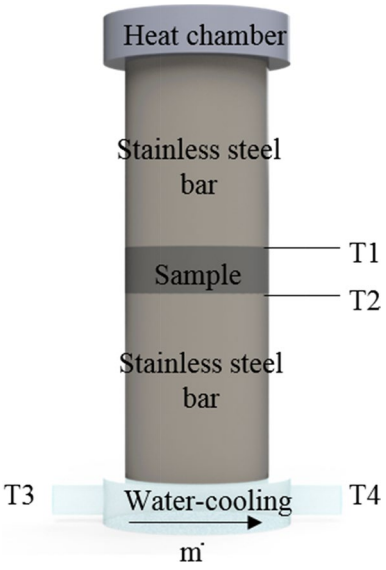

Fig. 4 Schematic diagram of thermal conductivity apparatus

calculated using Eqs. 1 and 2 [41] and then used to calculate the relative enhancement, $\kappa_{\text{enhancement}}$, using Eq. 3 [42]. This experiment was repeated three times, and then the average data was taken as a result. The standard error was also measured.

$$\kappa = (Q_{\text{w}} \times L)/[A \times (T_2 - T_1)], \tag{1}$$

where Q_{w} is the heat absorbed by the water cooler (kJ), L is the thickness of the sample (m), A is the area of the sample (m^2), and T_1 and T_2 are the temperatures at the top and bottom of the sample (K), respectively, as shown in Fig. 4. Q_{w} can be obtained as follows:

$$Q_{\text{w}} = \dot{m} \times C_{\text{p}} \times \Delta T. \tag{2}$$

$\dot{m}$ is the mass flow rate which is the amount of water-cooling flow (0.015 $\text{kg}\cdot\text{s}^{-1}$). C_{p} is the heat capacity of water (4.187 $\text{kJ}\cdot\text{kg}^{-1}\cdot\text{K}^{-1}$), and ΔT is the temperature difference between the water before and after heat is absorbed, $\text{T}_4 - \text{T}_3$ (K), as shown in Fig. 4.

$$\kappa_{\text{enhancement}} = \kappa/\kappa_0. \tag{3}$$

To determine the heat transfer rate of each sample, all the samples were heated at 60 °C. During the melting process, temperature increments were recorded over each interval of 60 s using a thermal camera (IR-TCM HD 1024, Jenoptik, Germany). A hot plate kept at a constant temperature of 60 °C was used to heat samples placed in a beaker, with melting performed for 900 s to determine the average final temperature and heat transfer from the gradient of the graph [43]. The hot plate was ensured to have a uniform temperature to provide consistent heat transfer to the sample. Nine points were taken from the calculation sample to obtain the most accurate average final temperature and temperature gradients. This experiment was repeated

Table 4 PV panels with different samples attached

PV name	Description	Type of PCM
PV1	conventional PV panel	None
PV2	PV panel with P	PCM
PV3	PV panel with PGS1	SNPCM
PV4	PV panel with PGS3	SNPCM
PV5	PV panel with PGS5	SNPCM

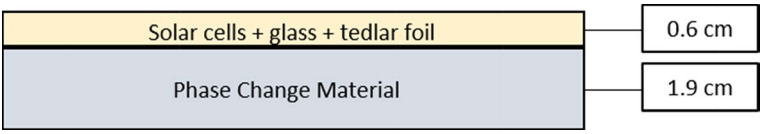

Fig. 5 The layer structure of the modified PV panel

three times, and then the average data was taken as a result. The standard error was also measured.

The total heat stored depended on the heat absorption of the material as it changed phase from solid to liquid or vice versa and the heat during the absence of phase changing. The total heat stored for each sample can be calculated from the following equation:

$$Q_s \times \left(m \times C_p \times \Delta T\right) + \left(m \times L\right), \tag{4}$$

where m is the mass of the sample (kg), C_p is its heat capacity (kJ·kg^{-1}·K^{-1}), ΔT is the temperature difference (K) between the initial and final sample temperatures at 0 and 900 s, meanwhile, L is the latent heat of the sample (kJ·kg^{-1}) respectively.

2.5 Modification of PV Panels

Each sample used in the study was fabricated before use as a PV panel coolant, i.e., each modified PV panel was filled with liquid sample material. The performances of five types of PV panels (Table 4) were compared; these included a conventional PV panel (PV1) and four other panels, designated PV2, PV3, PV4, and PV5, to which samples of PW, PGS1, PGS3, and PGS5 (from Table 3), respectively, were attached and subsequently cooled until they solidified. 1 kg of the sample was used, and the solidified PCM was left a 7-cm free space intended to accommodate volume expansion during the PCM melting [14]. Subsequently, an aluminum sheet was glued to the back of each PV panel with epoxy resin and then held in place. Figure 5 shows the layer structure of a modified solar PV panel with an overall thickness of 2.5 cm, comprising a 0.6 cm upper layer composed of protective glass, solar cell material, and Tedlar foil on top of a 1.9 cm thick layer PCM. The modification of this PV panel has been adapted and referred from the available literature [14].

2.6 On-site Evaluation of PV Panels Integrated with PCM and SNPCM

The performance of the PV panels developed in this study was evaluated based on three main parameters: solar irradiance, surface temperature, and ambient temperature. As shown in Fig. 6, these factors were assessed using an experimental setup in which the PV panels were connected to a K-type thermocouple that served as a temperature sensor and linked to a data logger (model OM-HL-EH-TC, Omega, China) that measured the panels' surface temperatures. Solar irradiance and ambient temperature were measured using a solar irradiance meter (model 2000r, the Seaward Solar Survey, UK). As shown in Fig. 6, the experiments were conducted outdoors at Universiti Teknologi Malaysia (UTM) Skudai, Malaysia, on days with high ambient temperature, high solar radiation, and low wind speed to ensure that the temperatures of the PV modules could rise to a required level. The high solar intensity, ambient temperature, and low wind speed produced high surface temperatures on the reference PV panels, enabling PV temperature regulation using PCM (PW) and SNPCM (PGS1, PGS3, PGS5). Experiments were conducted over 3 days, during which there was a peak solar irradiation of 1525 $W{\cdot}m^{-2}$, peak ambient temperatures of 41 °C, and wind speeds of up to 4.8 $m{\cdot}s^{-1}$.

Fig. 6 Photograph of the experimental setup

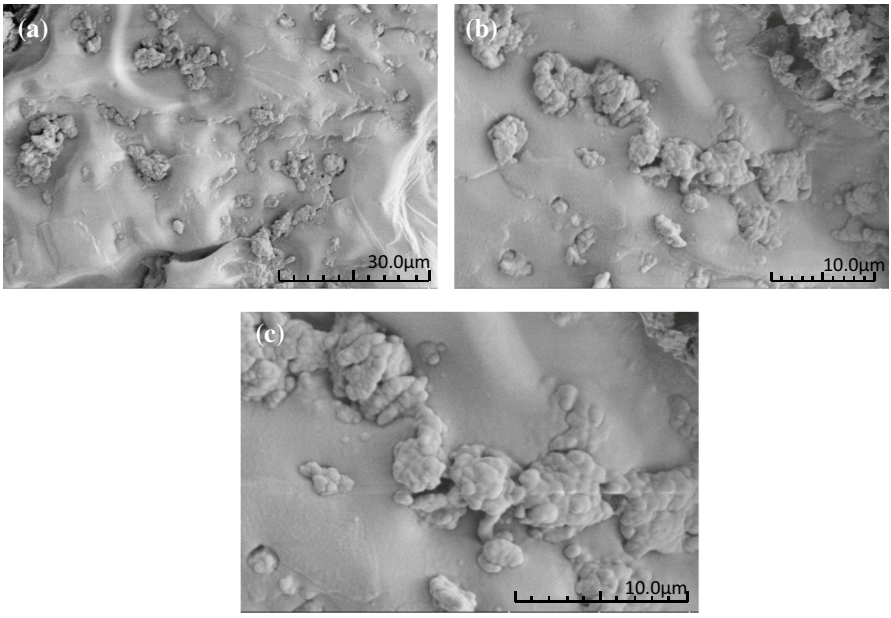

Fig. 7 FESEM images of PG5 at different magnifications: (a) × 1500, (b) × 3000, and (c) × 5000

3 Results and Discussion

3.1 Morphological Analysis and Physical Observation

Morphological analysis and physical observation of PW, NPCMs, and SNPCMs samples were studied using FESEM images and digital cameras. Figure 7 shows images of the dispersion and distribution of GNP within the PW matrix without SDBS (PG5) at different magnifications, revealing the agglomeration phenomenon within the sample. The sample underwent agglomeration due to relatively strong van der Waals forces of attraction among the NPs complemented by their Brownian motion [44, 45]. In addition, the repetitive process of melting and solidification causes the severe occurrence of agglomeration, which will further decrease the thermophysical properties of the NPCMs, reducing their ability to serve as a good coolant material [46].

Figure 8 shows the sample with the addition of SDBS (PGS5), confirming the stable and agglomeration-free sample. The surfactant reduced the surface tension [47], increasing the zeta potential and NPs stability and exhibit higher repulsive forces [48], which then weakens the van der Waals forces between NPs [49] and subsequently prevents the NPs from clustering or sticking together, thereby mitigating agglomeration [50]. The addition of SDBS helped the GNP to disperse completely and uniformly throughout the PW. This factor is the main factor contributing to enhancing all thermophysical properties of the samples investigated in this study.

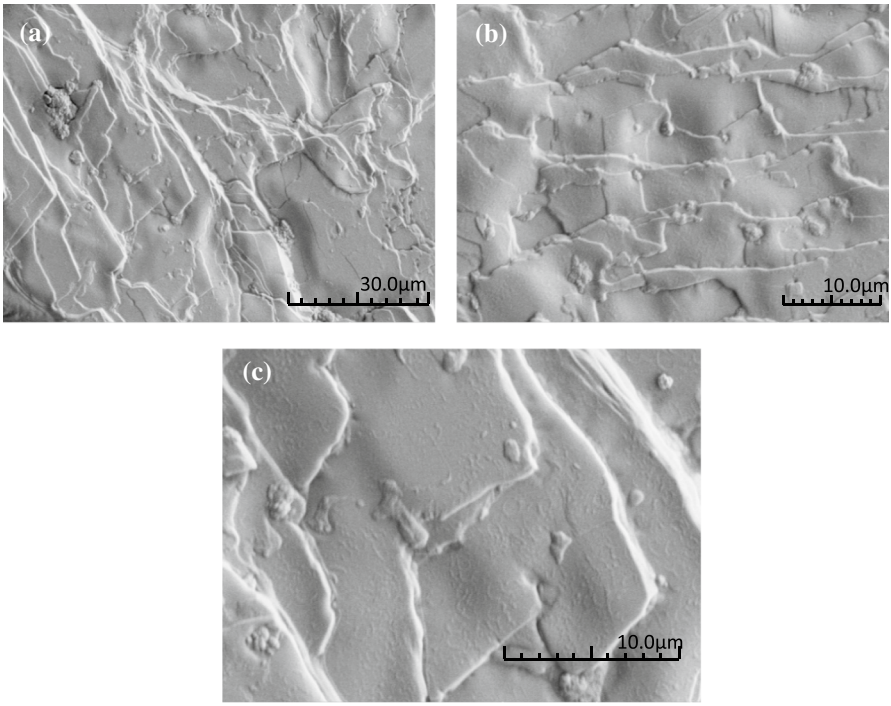

Fig. 8 FESEM images of PGS5 at different magnifications: (a) × 1500, (b) × 3000, and (c) × 5000

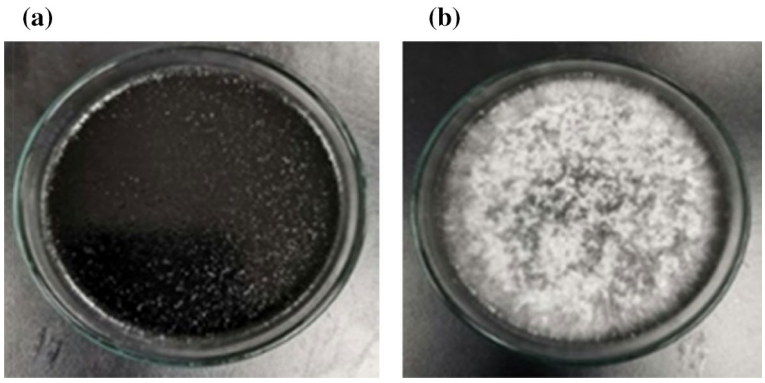

Fig. 9 The solidifying process of PG5 after (a) 60 s and (b) 3600 s

Figures 9 and 10 show the solidifying process of both NPCMs, with and without the addition of SDBS. Figure 9 indicates that NPCMs (PG5) underwent sedimentation without surfactant due to GNP agglomeration (as mentioned in morphological analysis). On the other hand, the addition of SDBS in the NPCMs (PGS5) reduced the sedimentation due to less agglomeration, as seen in Fig. 10.

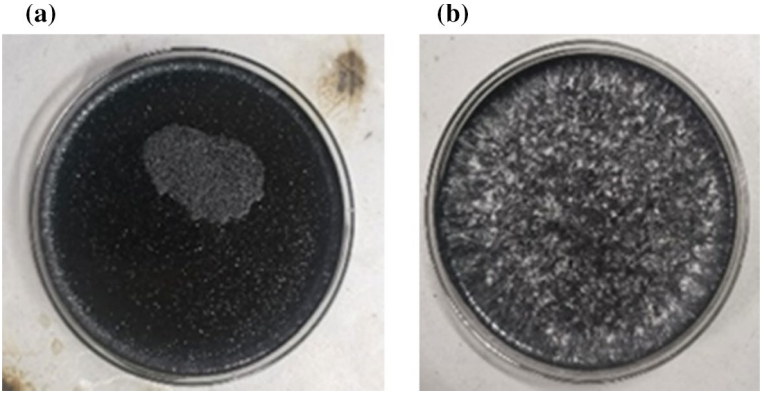

Fig. 10 The solidifying process of PGS5 after (a) 60 s and (b) 3600 s

Table 5 Melting, solidification time of samples, and percentages of sample's time-saving relative to PW's time

Sample	Solidifying time (s)	Melting time (s)
PW	4321	761
PG1	3896 (9.84%)	707 (7.09%)
PG3	3742 (13.40%)	658 (13.53%)
PG5	3600 (16.69%)	609 (19.97%)
PGS1	3591 (16.89%)	568 (25.36%)
PGS3	3552 (17.80%)	550 (27.72%)
PGS5	3142 (37.52%)	332 (56.30%)

3.2 Thermophysical Property

Table 5 shows the difference in melting and solidifying time of samples relative to the PW time, in which PGS5 solidified the fastest (3142 s), i.e., 37.5% faster than PW (4321 s). A similar pattern can also be observed for the melting time of the PGS5 sample (332 s), 56.3% improvement compared to PW (761 s). In general, adding a higher amount of GNP with SDBS would improve the base material's charging-and-discharging period. SDBS is believed to facilitate the dispersal of NPs [28, 32, 35] with fewer agglomerates, increasing the amount of NPs with a high specific surface area available inside the PCMs for interaction. Moreover, higher GNP content helps to overcome the forces of attraction between particles during solidifying or melting process, resulting in an improved charging-and-discharging rate. A shorter charging and discharging rate indicate good heat transfer performance in PCMs, which is important when considering the cooling PV module.

Figure 11 shows the differential scanning calorimetry (DSC) curves for the samples. The addition of GNP and SDBS altered the endothermic and exothermic graphs, as evidenced by the decreasing strength of the endothermic and exothermic peaks. PW showed the broadest endothermic and exothermic peaks. In contrast, the

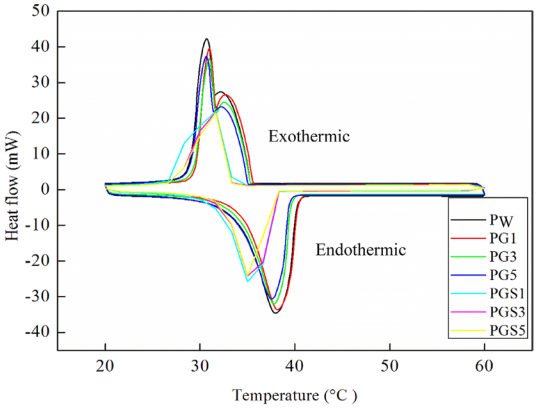

Fig. 11 DSC curves of all samples

Table 6 DSC analysis results

Sample	Solidification temperature (°C)	Melting temperature (°C)	Latent heat ($kJ \cdot kg^{-1}$)	Specific heat capacity ($kJ \cdot kg^{-1} \cdot K^{-1}$)
PW	31.00	35.00	160.00	2.00
PG1	31.97	36.89	190.79	3.02
PG3	31.74	36.67	196.43	3.17
PG5	32.14	37.16	197.29	3.18
PGS1	30.41	35.02	216.72	3.31
PGS3	30.11	34.99	228.49	3.32
PGS5	30.39	35.19	229.12	3.39

PGS5 sample showed the narrowest peaks, suggesting that the amount of PW in the samples decreases as the weights of GNP and SDBS increase.

Table 6 indicates DSC analysis results, and it can be seen that GNP addition to PW did not affect the melting temperature, as the maximum deviation from the melting point of PW was only 6.27%. The melting temperatures of the fabricated samples were in the range of 34.99–37.16 °C. The solidification temperature shows a similar trend; the highest percentage difference was between solidification temperatures of PW and other samples at 3.7%. The solidification temperatures of the samples were in the range of 30.11–32.14 °C. In general, the addition of GNP with or without SDBS did not seem to affect the melting or solidification temperature—a result that agrees with the findings of other studies [51]. Since PV panel operating temperature is around 25 °C, melting and solidification points are important parameters for a PCMs to operate according to the melting and solidification temperature. Thus it would be preferred for the prepared samples to have melting and solidification temperature in the desired operating temperature of the PW.

From Table 6, it can be observed that the latent heat of PW was the lowest (160.0 $kJ \cdot kg^{-1}$). In contrast, PGS5 had the highest latent heat (229.1 $kJ \cdot kg^{-1}$);

impregnation of GNP and presence of surfactant leads to increment in latent heat. As mentioned before, SDBS facilitates the dispersion of NPs, resulting in more NPs with an enhanced surface area are available for interaction. Meanwhile, more particles are available for heat transfer to melt the PCM with a higher amount of NPs. Therefore, high latent heat is an important parameter for a PCM to ensure a maximum heat absorption of PCM before it becomes fully liquid and dissipates heat back to the PV panel.

It can be observed that PGS5 shows the highest heat capacity (3.39 $kJ \cdot kg^{-1}$) compared to all the other samples. On the other hand, PW shows the lowest specific heat capacity (2.0 $kJ \cdot kg^{-1}$). It can be observed that the specific heat capacity increase with the presence of surfactant and the increasing amount of NPs added. This can be related to reducing agglomeration due to the addition of SDBS, which increases the amount of NPs with a high specific surface area. The specific heat capacity increases with NPs due to higher NPs, resulting in a higher amount of particles available for heat transfer to occur, increasing the specific heat capacity since heat capacity is the amount of heat required to raise 1 °C of heat sample's heat temperature. Specific heat capacity is also an important parameter for good PCMs. A high specific heat capacity will ensure minimum sensible heating.

Figure 12 shows the thermal conductivity of all the samples. The thermal conductivity improved the highest with surfactant and GNP concentration at 5 wt%, PGS5 (9.08 $W \cdot m^{-1} \cdot K^{-1}$). PW showed the lowest thermal conductivity with 0.35 $W \cdot m^{-1} \cdot K^{-1}$. Overall, a higher amount of GNP with the addition of SDBS resulted in a greater increase in thermal conductivity.

Meanwhile, a high GNP leads to greater interaction between the PW matrix and GNP, providing more particles available for heat transfer, thus enhancing thermal conductivity [29]. These results also indicate that the thermal conductivity depends on the percentage of NPs' weight and the presence of SDBS. From a PV cooling perspective, it is preferred to have a high value for thermal conductivity, as it indicates that the sample is a good conductor of heat and efficient in transferring heat, one of the essential characteristics of becoming a good PV coolant [14].

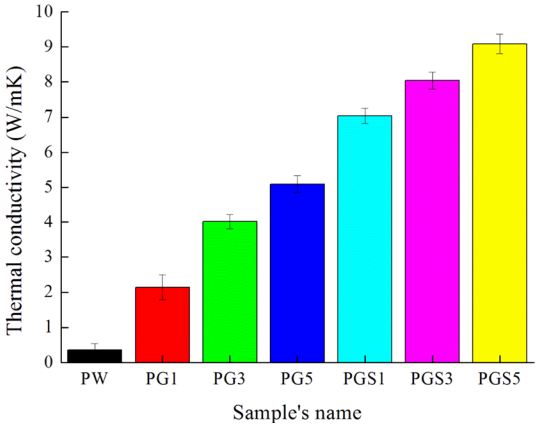

Fig. 12 Thermal conductivities of fabricated samples

Table 7 Relative enhancements in thermal conductivity

References	Relative enhancement in thermal conductivity	Percentages by weight of GNP (wt%)
This study: PGS1	19.50	1
This study: PGS5	25.94	5
Chang et al. [52]	6.38	15
Zabihi and Araghi [53]	1.93	4
Praveen et al. [54]	1.97	3
Liu and Rao [55]	1.59	2
Kumar et al. [56]	1.66	2
Liu et al. [57]	1.51	2.5

Table 7 compares the relative enhancements in thermal conductivity achieved in various studies. The high relative enhancement of conductivity demonstrated by the PGS5 sample is further confirmed by Eq. 3, which gives a value of 25.94. Furthermore, even the PGS1 sample, which had the lowest percentage by weight of SDBS in this study, demonstrated a substantially higher relative enhancement of thermal conductivity (19.5) than the factor of 6.4 at 15 wt% reported in Chang et al. [52]. Thus, the results of this study indicate that the introduction of SDBS in the NPCMs matrix, even at small percentages by weight (i.e., 1 wt%), can substantially enhance thermal conductivity. Thus, indicating the importance of SDBS addition.

The obtained melting profiles were then combined into one average melting profile, as shown in Fig. 13. Figure 13 shows the average temperature of the melting profile for various samples, from which the final melting temperature and heat transfer rate can be obtained. The PGS5 sample exhibited the highest heat transfer rate (1.96 $K{\cdot}s^{-1}$), i.e., which is also shown by the steepest slope of PGS5. Meanwhile, PW shows the lowest heat transfer rate (1.13 $K{\cdot}s^{-1}$), shown by the PW's least steep slope. Overall, the samples with SDBS (PGS1, PGS3, and PGS5) exhibited higher heat transfer rates than those without SDBS (PG1, PG3, PG5, and P) and higher GNP in higher heat transfer rates. This is due to

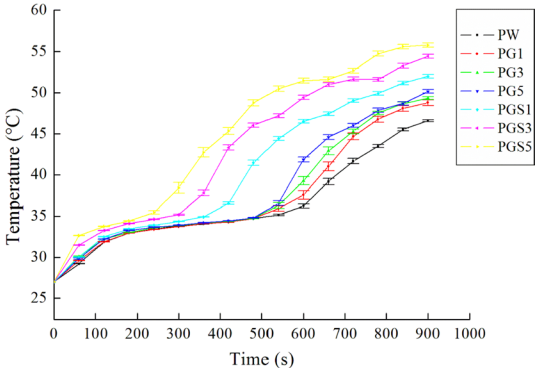

Fig. 13 Melting profiles of average temperatures for various samples

Table 8 Total heat stored of all samples

Materials	Heat source (°C)	Mass (kg)	C_p (kJ·kg^{-1}·K^{-1})	T_f (°C)	T_i (°C)	Latent heat (kJ·kg^{-1})	Q_s (kJ)
PW	60	0.0112	2.00	46.58	27	160.00	2.23
PG1	60	0.0112	3.02	48.79	27	190.79	2.87
PG3	60	0.0112	3.17	49.34	27	196.43	2.99
PG5	60	0.0112	3.18	50.15	27	197.29	3.03
PGS1	60	0.0112	3.31	52.00	27	216.72	3.35
PGS3	60	0.0112	3.32	54.42	27	228.49	3.58
PGS5	60	0.0112	3.39	55.79	27	229.12	3.66

Table 9 PV panel performance

PV names	PV surface temperature (°C)	Temperature reduction (°C)
PV1	71.5	0
PV2	63.2	9.2
PV3	48.6	22.9
PV4	45.6	25.9
PV5	39.9	31.6

SDBS reduce the agglomeration of NPs. In addition, the high amount of NPs improve the heat transfer rate due to the small size of NPs resulting in a higher specific surface area. Therefore, more particles available for heat transfer occur with a high surface area, which increases the heat transfer rate. These findings of heat transfer improvement upon the addition of SDBS agree with those reported in previous studies [32, 35]. Considering that thermal conductivity is the heat transfer rate through a unit thickness of a material per unit area and per unit temperature difference [58], PGS5 exhibited the highest thermal conductivity, agreeing with the results shown in Sect. 3.2.3. Therefore, it is important to analyze the heat transfer rate to find the total heat stored in a sample.

Table 8 shows the performance of the PW and various fabricated samples based on the total heat stored, as defined by Eq. 4. The specific heat capacity was obtained from Table 6, while the final and initial melting temperature was obtained from Fig. 13. Based on Table 8, it can be observed that PGS5 could store the heat ($Q_s = 3.66$ kJ) better than all other samples. Meanwhile, PW could store the least heat (2.23 kJ). Thus, it can be concluded that PGS5 is better than all the other samples because PGS5 can store more energy as a PV coolant. Therefore, total heat stored indicates the amount of heat PCM can store, an important parameter to ensure a good PV panel coolant.

3.3 On-site Evaluation of PV Panels Integrated with PCMs and SNPCMs

Table 9 lists the PV surface temperature and reductions in the PV temperature under irradiance obtained by the corresponding samples. PV5 achieved the highest temperature reduction (31.6 °C), and increasing GNP with SDBS improved temperature reduction. In addition, the PGS5 used in PV5 exhibited the highest increase in thermal conductivity (9.97 $W{\cdot}m^{-1}{\cdot}K^{-1}$), which led to the optimal heat absorption for cooling the PV panel. By contrast, PV2 exhibited the lowest temperature reduction due to the low thermal conductivity of PW applied to the back of the sample. These results further demonstrate the effective PV coolant characteristics of PGS5.

Figure 14a shows the solar radiation intensity during the daytime over the 3 days of the irradiance assessment, during which the highest solar irradiances were attained before noon, although the specific values slightly fluctuated during the day. These fluctuations can be accounted for by several factors, including cloud shading and changes in ground surface reflectivity. Cloud shadow is a common phenomenon in Malaysia because the country is near the equator, where the climate is typically tropical, with high temperatures and humidity throughout the year. Figure 14b shows that the ambient temperature also fluctuated throughout

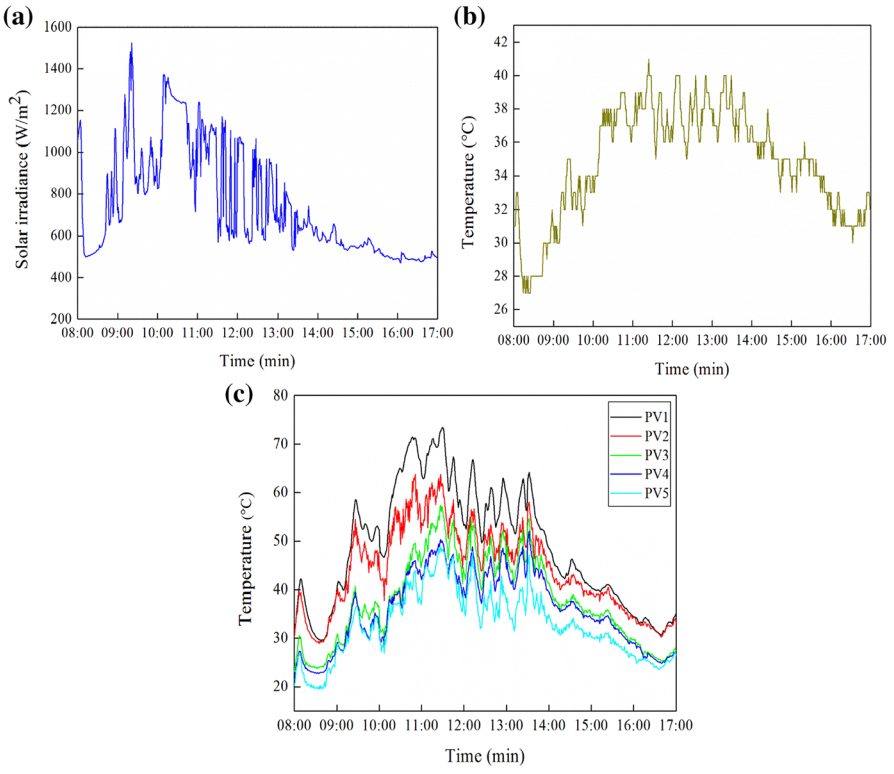

Fig. 14 (a) Solar irradiance. (b) Ambient temperature. (c) PV surface temperatures

the day, with the highest temperatures occurring between 12:00 and 13:00. The wind speed over the three days varied between 2.2 and 4.7 $m \cdot s^{-1}$, resulting in higher temperatures at the front surface of the PV panel, which in turn increased the amount of heat stored in the panel and the resulting outward heat transfer. The addition of PCM and SNPCM to a PV panel enhances the absorption, storage, and transference of heat from the panel, thereby reducing the PV panel temperature while creating a high open-circuit voltage (V_{oc}) that enhances the output power of the panel relative to that of a conventional PV panel.

Figure 14c shows the PV panels' surface temperatures throughout the day, averaged over three days. Over 2.5 h, the average front surface temperature of PV1 increased rapidly from 32.2 °C at 08:00 to 71.5 °C at 10:47, reaching a peak temperature of 73.5 °C at 11:30; the temperature profiles of the other PV panels followed similar trends. The peak average temperature of PV1 corresponded to the peak ambient temperature of 41 °C and high solar irradiance of 1115 $W \cdot m^{-2}$ at 11:24. Although the highest solar irradiance value of 1525 $W \cdot m^{-2}$ occurred at 09:21, the temperature of PV1 at that time was not at its highest because of the low ambient temperature and high wind speed. The increase in the temperature of PV1 between 08:00 and 11:30 can be attributed to the increases in incident solar radiation (Fig. 14a) and ambient temperature (Fig. 14b). The temperature of PV1 then decreased to 60.3 °C; this temperature was maintained for approximately 2 h (between 11:39 and 13:39) before rapidly dropping to 42.6 °C at 1419 h. The relative stability in the temperature of PV1 between 11:39 and 13:39 can be attributed to the heat balance of the panel reaching a steady state at which the input solar radiation was equal to the sum of heat losses; the rapid drop of the PV temperature after 14:19 is attributable to the combined effects of (i) the reduction of the incoming input heat to the panel as a result of the decrease in the solar radiation intensity (Fig. 14a), (ii) the reduction of the ambient temperature (Fig. 14b), and (iii) an increase in the amount of heat transferred from the panel to the ambient air arising from a combination of a decrease in the ambient temperature and an increase in the wind speed. In general, the temperature profile of PV1 followed the ambient temperature profile, which accounted for the daily temperature fluctuations. Changes in the wind speed also cause fluctuations in the PV panel temperature profile throughout the day.

The other PV panels, i.e., PV2, PV3, PV4, and PV5, followed the same trend as PV1, with PV5 experiencing the highest reduction of the PV temperature, followed by PV4, PV3, PV2, and PV1 (Table 9). Overall, PGS5 outperformed the other samples in terms of the PV panel coolant capability, as it experienced the highest PV temperature reduction of 31.6 °C (Table 9). In general, these results agree well with the experimental thermophysical enhancement of the samples.

Increased GNP content with the addition of SDBS enhanced the thermal conductivity of the PCMs, allowing heat transfer to occur at a higher rate. The high thermal conductivity of PGS5 in PV5 facilitated the rate of phase change in the material, enabling it to perform better as a storage system and more effectively reduce the PV temperature. The high degree of temperature reduction occurring in PV5 corresponds to a high open-circuit voltage (V_{oc}) and, consequently, an enhanced output power, proportional to V_{oc} [5]. Although the surface temperature of PV5 remained

Table 10 Comparison of highest PV-NPCM temperature reductions achieved in various studies

References	Highest PV temperature reduction (°C)
This study: PV5	31.6
Nada et al. [5]	18
Salem et al. [60]	12
Siahkamari et al. [61]	26
Abdelrahman et al. [59]	39

the lowest and the panel produced the highest output power, further investigation is required to validate the reliability of the PV coolant developed in this study.

Table 10 compares the highest PV temperature reductions obtained in various studies. In Nada et al. [5], integrated PV panels containing PCM and PCM/Al_2O_3 reduced the PV temperature by 8.1 °C and 10.6 °C, respectively, improving the efficiency by 5.7 and 13.2%, respectively. In Abdelrahman et al. [59], PV panel cases were integrated with PCM and PCM/Al_2O_3 at various percentages of the weight of Al_2O_3 ranging from 0.11 to 0.77% cylindrical fins were used as heat sinks and thermal conductivity enhancers (TCEs). These enhancements reduced the PV temperature by 20.0–46.3%. The addition of Al_2O_3 increased the PV temperature reduction to 52.3%, whereas the integration of nano-enhanced PCM and microfins reduced the PV temperature by 12.5 °C. Salem et al. [60] tested the use of square-tube thermal collectors filled with PCM/Al_2O_3 composite (from 0 to 1 wt%) at various volumes (0, 25, 50, 75, and 100%) with non-filled PCM tubes used to circulate water. The results showed that the compound technique (Al_2O_3/PCM mixture + water) applying Al_2O_3 at 1 wt% achieved the best results relative to cooling with 100% water. Siahkamari et al. [61] reported on PCM and PCM/CuO testing and revealed that the PCM-with-CuO mixture reduced PV temperature more effectively than a PW mixture. Although the maximum temperature reduction obtained here ranked only second-highest (31.6 °C) among the surveyed studies, the relative ease of synthesis and easier integration with PV panels make the sample a potential candidate in PV module cooling.

4 Conclusion

An extensive study was conducted to assess the improvement of thermophysical properties of NPCMs with an additional surfactant (SDBS). Thermophysical properties such as charging and discharging rate, phase change temperature, latent heat, specific heat capacity, thermal conductivity, and total heat stored of the PW, NPCMs, and SNPCMs were investigated experimentally. Based on the results, the following conclusions can be made;

- SDBS addition in the PCMs matrix proven to enhance the thermophysical properties of PCM.

- PGS5 was found to possess the optimal characteristics, representative of a good PCM, with less agglomeration, shortest charging and discharging time, highest latent heat (229.12 $kJ{\cdot}kg^{-1}$), specific heat capacity (3.39 $kJ{\cdot}kg^{-1}{\cdot}K^{-1}$), thermal conductivity (9.08 $W{\cdot}m^{-1}{\cdot}K^{-1}$), heat transfer rate (1.96 $K{\cdot}s^{-1}$) and total heat stored (3.66 kJ).

Thus, it can be concluded that a higher percentage of GNP weight NPs with SDBS improve the dispersion and thermophysical properties of PW. As a PV panel coolant, PGS5 is favorable. It has a better charging and discharging rate and heat transfer, the highest latent heat, heat capacity, and the largest thermal conductivity. In addition, it can store the most amount of heat compared to all the other samples. This result is further supported by the temperature reduction profile shown by the PV modules obtained from the on-site evaluation conducted. Easy material synthesis, added with an easier integration method with PV module, makes it a potential candidate for PV module cooling.

Acknowledgements This work was supported by the Malaysian Ministry of Higher Education and UTM through the Research University Grant (GUP) Vot. No. Q.J130000.2651.15J79

References

1. *The effect of temperature on solar panel performance*. https://solarcalculator.com.au/solar-panel-temperature/
2. S. Krauter, Increased electrical yield via water flow over the front of photovoltaic panels. Sol. Energy Mater. Sol. Cells **82**, 131–137 (2004)
3. S. Krauter et al., Combined photovoltaic and solar thermal systems for facade integration and building insulation. Sol. Energy **67**, 239–248 (1999)
4. D. Du, J. Darkwa, G. Kokogiannakis, Thermal management systems for photovoltaics (PV) installations: a critical review. Sol. Energy **97**, 238–254 (2013)
5. S.A. Nada, D.H. El-Nagar, H.M.S. Hussein, Improving the thermal regulation and efficiency enhancement of PCM-integrated PV modules using nano particles. Energy Convers. Manag. **166**, 735–743 (2018)
6. S. Sharma et al., Nano-enhanced phase change material for thermal management of BICPV. Appl. Energy **208**, 719–733 (2017)
7. R. Stropnik, U. Stritih, Increasing the efficiency of PV panel with the use of PCM. Renew. Energy **97**, 671–679 (2016)
8. J. Zhao, P. Lv, Z. Rao, Experimental study on the thermal management performance of phase change material coupled with heat pipe for cylindrical power battery pack. Exp. Therm. Fluid Sci. **82**, 182–188 (2017)
9. A. Zehri, et al., High porosity and light weight graphene foam heat sink and phase change material container for thermal management. Nanotechnology **31**, 424003 (2020)
10. S. Mo et al., Thermophysical properties of a novel nanoencapsulated phase change material. Int. J. Thermophys. **41**, 68 (2020)
11. G. Wang et al., Impact evaluation of cold heat transfer fluid temperature on heat storage and mechanical behaviours of an energy storage system using phase-change material. Int. J. Thermophys. **42**, 64 (2021)
12. Z. Zhang, Z. Ci, T. Zhang, Heat-storage performance optimization for packed bed using cascaded PCMs capsules. Int. J. Thermophys. **42**, 72 (2021)
13. H.F. Abbasov, The effective thermal conductivity of composite phase change materials with open-cellular metal foams. Int. J. Thermophys. **41**, 164 (2020)

14. A. Hasan et al., Yearly energy performance of a photovoltaic-phase change material (PV-PCM) system in hot climate. Sol. Energy **146**, 417–429 (2017)
15. A.-M.N.M. Al-Ajeely, M.T. Chaichan, S.H. Kamel, Thermal conductivity enhancement by using nano-material in phase change material for latent heat thermal energy storage systems. Saussurea **5**, 48–55 (2015)
16. B. Kamkari, D. Groulx, Experimental investigation of melting behaviour of phase change material in finned rectangular enclosures under different inclination angles. Exp. Therm. Fluid Sci. **97**, 94–108 (2018)
17. S. Sharma et al., Performance enhancement of a building-integrated concentrating photovoltaic system using phase change material. Sol. Energy Mater. Sol. Cells **149**, 29–39 (2016)
18. A. Hassan et al., Energy and cost saving of a photovoltaic-phase change materials (PV-PCM) system through temperature regulation and performance enhancement of photovoltaics. Energies **7**, 1318–1331 (2014)
19. A. Hasan et al., Increased photovoltaic performance through temperature regulation by phase change materials: materials comparison in different climates. Sol. Energy **115**, 264–276 (2015)
20. M.M. Islam et al., Recent progresses and achievements in photovoltaic-phase change material technology: a review with special treatment on photovoltaic thermal-phase change material systems. Energy Convers. Manag. **126**, 177–204 (2016)
21. S. Maiti et al., Self regulation of photovoltaic module temperature in V-trough using a metal–wax composite phase change matrix. Sol. Energy **85**, 1805–1816 (2011)
22. F. Hachem et al., Improving the performance of photovoltaic cells using pure and combined phase change materials—experiments and transient energy balance. Renew. Energy **107**, 567–575 (2017)
23. Z. Luo et al., Numerical and experimental study on temperature control of solar panels with form-stable paraffin/expanded graphite composite PCM. Energy Convers. Manag. **149**, 416–423 (2017)
24. A.E. Kabeel, et al., Experimental study on tubular solar still using graphene oxide nano particles in phase change material (NPCM's) for fresh water production. J. Energy Storage **28**, 101204 (2020)
25. S. Sami, N. Etesami, Improving thermal characteristics and stability of phase change material containing TiO_2 nanoparticles after thermal cycles for energy storage. Appl. Therm. Eng. **124**, 346–352 (2017)
26. V. Saydam, X. Duan, Dispersing different nanoparticles in paraffin wax as enhanced phase change materials: a study on the stability issue. J. Therm. Anal. Calorim. **135**, 1135–1144 (2018)
27. A. Chibani, S. Merouani, Acceleration of heat transfer and melting rate of a phase change material by nanoparticles addition at low concentrations. Int. J. Thermophys. **42**, 66 (2021)
28. A. Babapoor, G. Karimi, Thermal properties measurement and heat storage analysis of paraffin nanoparticles composites phase change material: comparison and optimization. Appl. Therm. Eng. **90**, 945–951 (2015)
29. N. Ali, J.A. Teixeira, A. Addali, A review on nanofluids: fabrication, stability, and thermophysical properties. J. Nanomater. **2018**, 6978130 (2018)
30. A. Sánchez-Coronilla et al., Experimental and theoretical analysis of NiO nanofluids in presence of surfactants. J. Mol. Liq. **252**, 211–217 (2018)
31. S. Chakraborty et al., effect of surfactant on thermo-physical properties and spray cooling heat transfer performance of Cu–Zn–Al LDH nanofluid. Appl. Clay Sci. **168**, 43–55 (2019)
32. A.H.A. Al-Waeli et al., evaluation and analysis of nanofluid and surfactant impact on photovoltaic–thermal systems. Case Stud. Therm. Eng. **13**, 100392 (2019)
33. Y. Zhai et al., evaluation of surfactant on stability and thermal performance of Al_2O_3–ethylene glycol (EG) nanofluids. Powder Technol. **343**, 215–224 (2019)
34. S. Hashempour, M.H. Vakili, Preparation and characterisation of nano enhanced phase change material by adding carbon nano tubes to butyl stearate. J. Exp. Nanosci. **13**, 188–198 (2018)
35. R.K. Sharma et al., Thermal properties and heat storage analysis of palmitic acid–TiO_2 composite as nano-enhanced organic phase change material (NEOPCM). Appl. Therm. Eng. **99**, 1254–1262 (2016)
36. M. Nourani et al., Thermal behavior of paraffin-nano-Al_2O_3 stabilized by sodium stearoyl lactylate as a stable phase change material with high thermal conductivity. Renew. Energy **88**, 474–482 (2016)
37. N. Şahan, M. Fois, H. Paksoy, Improving thermal conductivity phase change materials—a study of paraffin nanomagnetite composites. Sol. Energy Mater. Sol. Cells **137**, 61–67 (2015)
38. A.R. Vakhshouri, *Paraffin as Phase Change Material* (IntechOpen, London, 2019)

39. H. Cortés et al., Non-ionic surfactants for stabilization of polymeric nanoparticles for biomedical uses. Materials **14**, 3197 (2021)
40. N.H. Muhd Zaimi et al., *Effect of Graphene Oxide Nanoparticles on Thermal Properties of Paraffin Wax* (Springer, Singapore, 2020)
41. Y. Al Abdallat, J. Yamin, Manufacturing and testing of light-weight foamed concrete: experimental results. Mod. Appl. Sci. **13**, 128 (2019)
42. M. Kenisarin, et al., Enhancing thermal conductivity of paraffin wax 53–57 °C using expanded graphite. Sol. Energy Mater. Sol. Cells **200**, 110026 (2019)
43. H. Ambarita, et al., Experimental study on melting and solidification of phase change material thermal storage. IOP Conf. Ser. Mater. Sci. Eng. **180**, 012030 (2017)
44. M. Amin et al., Thermal properties of beeswax/graphene phase change material as energy storage for building applications. Appl. Therm. Eng. **112**, 273–280 (2017)
45. M. Pasupathi et al., Characterization of hybrid-nano/paraffin organic phase change material for thermal energy storage applications in solar thermal systems. Energies **13**, 5079 (2020)
46. A.A. Shamsuri, S.NMd. Jamil, A short review on the effect of surfactants on the mechanico-thermal properties of polymer nanocomposites. Appl. Sci. **10**, 4867 (2020)
47. S.U. Ilyas, S. Ridha, F.A. Abdul Kareem, Dispersion stability and surface tension of SDS-stabilized saline nanofluids with graphene nanoplatelets. Colloids Surf. A **592**, 124584 (2020)
48. S.L. Tariq, et al., Nanoparticles enhanced phase change materials (NePCMs)—a recent review. Appl. Therm. Eng. **176**, 115305 (2020)
49. X.-X. Tian et al., Competition between intermolecular forces of adhesion and cohesion in the presence of graphene nanoparticles: investigation of graphene nanosheets/ethylene glycol surface tension. J. Mol. Liq. **311**, 113329 (2020)
50. Z. Zhao, et al., Fluidization of nanoparticle agglomerates assisted by combining vibration and stirring methods. Chem. Eng. J. **388**, 124213 (2020)
51. N. Putra, E. Prawiro, M. Amin, Thermal properties of beeswax/CuO nano phase-change material used for thermal energy storage. Int. J. Technol. (2016). https://doi.org/10.14716/IJTECH.V7I2.2976
52. T.-C. Chang et al., PCM based heat sinks of paraffin/nanoplatelet graphite composite for thermal management of IGBT. Appl. Therm. Eng. **112**, 1129–1136 (2017)
53. Z. Zabihi, H. Araghi, Effect of functional groups on thermal conductivity of graphene/paraffin nanocomposite. Phys. Lett. A **380**, 3828–3831 (2016)
54. B. Praveen, S. Suresh, V. Pethurajan, Heat transfer performance of graphene nano-platelets laden micro-encapsulated PCM with polymer shell for thermal energy storage based heat sink. Appl. Therm. Eng. **156**, 237–249 (2019)
55. X. Liu, Z. Rao, Experimental study on the thermal performance of graphene and exfoliated graphite sheet for thermal energy storage phase change material. Thermochim. Acta **647**, 15–21 (2017)
56. K. Kumar et al., Experimental investigation of grapheme–paraffin wax nanocomposites for thermal energy storage. Mater. Today Proc. **18**, 5158–5163 (2019)
57. C. Liu et al., Experimental study on the phase change and thermal properties of paraffin/carbon materials based thermal energy storage materials. Phase Transit. **90**, 717–731 (2017)
58. M. Bahrami, *Steady Conduction Heat Transfer*. https://www.sfu.ca/~mbahrami/ENSC%20388/Notes/Staedy%20Conduction%20Heat%20Transfer.pdf. Accessed 10 May 2021
59. H.E. Abdelrahman et al., Performance enhancement of photovoltaic cells by changing configuration and using PCM (RT35HC) with nanoparticles Al_2O_3. Sol. Energy **177**, 665–671 (2019)
60. M.R. Salem et al., Performance enhancement of the photovoltaic cells using Al_2O_3/PCM mixture and/or water cooling-techniques. Renew. Energy **138**, 876–890 (2019)
61. L. Siahkamari et al., Experimental investigation on using a novel phase change material (PCM) in micro structure photovoltaic cooling system. Int. Commun. Heat Mass Transf. **100**, 60–66 (2019)

Authors and Affiliations

Nurul Humaira Muhd Zaimi[1] · Amirjan Nawabjan[1] · Shaharin Fadzli Abd Rahman[2] · Siti Maherah Hussin[1] · Siti Nur Nashya Azlika Hamidon[1]

✉ Amirjan Nawabjan
amirjan@utm.my

[1] Centre of Electrical Energy Systems (CEES), Institute of Future Energy, School of Electrical Engineering, Faculty of Engineering, Universiti Teknologi Malaysia (UTM), 81310 Johor Baharu, Johor, Malaysia

[2] School of Electrical Engineering, Faculty of Engineering, Universiti Teknologi Malaysia (UTM), 81310 Johor Baharu, Johor, Malaysia